THE JOURNAL OF PHYSICAL CHEMISTRY B

Article

pubs.acs.org/JPCB

Photochemistry of a Bacterial Photosynthetic Reaction Center Missing the Initial Bacteriochlorophyll Electron Acceptor

Brett Carter,[†] Steven G. Boxer,[†] Dewey Holten,[‡] and Christine Kirmaier*[,‡]

[†]Department of Chemistry, Stanford University, Stanford, California 94305-5080, United States

[‡]Department of Chemistry, Washington University, St. Louis, Missouri 63130-4899, United States

ABSTRACT: A novel chromophore composition of the bacterial photosynthetic reaction center (RC) has been discovered: RCs lacking the L-side monomeric bacteriochlorophyll chromophore result from mutation of the native isoleucine at M204 to glutamine in *Rhodobacter capsulatus*. This conclusion is obtained from 77 K UV−vis spectroscopy and pigment extractions of the I(M204)Q mutant and seven variants containing the I(M204)Q plus other mutations. The oxidation potential of the primary electron donor P (a dimer of bacteriochlorophylls) was measured for three of the mutants and found to be 50−65 mV lower than in wild-type RCs. Ultrafast transient absorption measurements reveal (minimally) two subpopulations of P* that have distinct lifetimes and photochemical outcomes for all mutants containing I(M204)Q. In one subpopulation P* decays solely by internal conversion to the ground state. In the other subpopulation P* decays by electron transfer to the normally inactive M-side bacteriopheophytin (H_M) in competition with internal conversion to the ground state. When a Tyr residue is substituted for the native Phe at L181 near the M-side monomeric bacteriochlorophyll (B_M), the rate of electron transfer to H_M is increased about 4-fold.

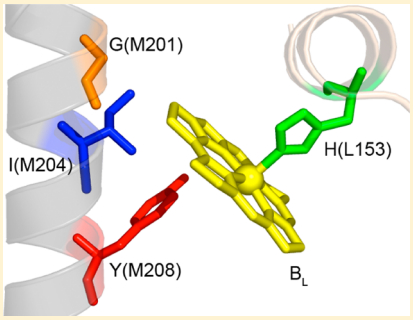

INTRODUCTION

The initial light driven electron transfer (ET) reaction in bacterial photosynthetic reaction centers (RCs) is mediated by a monomeric bacteriochlorophyll (BChl), denoted B_L, which lies between the special pair primary electron donor, P, consisting of two BChls and the bacteriopheophytin (BPh) electron acceptor H_L on the L-side of the RC (Figure 1). The role of the BChl in the B_L site in initial charge separation has been much debated. It has been difficult to observe the putative intermediate $P^+B_L^-$ in unmodified RCs since the decay time of this species to form $P^+H_L^-$ (~0.5 to 4 ps) is shorter than or only slightly longer than the time scale of its formation from P* (3−4 ps).[1,2] Recently, we trapped the $P^+B_L^-$ intermediate in two variants of the H_L-less D_{LL} mutant[3] and showed that this state has an inherent lifetime (i.e., its lifetime in the absence of ET to H_L) on the order of several hundred picoseconds.[4] These results also indicated that $P^+B_L^-$ lies below P* in free energy in these two mutant RCs.

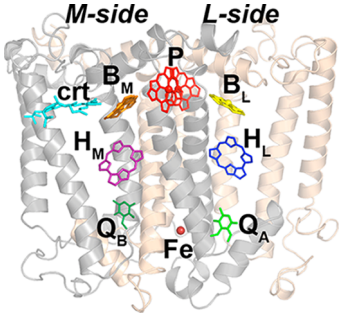

Figure 1. Reaction center with the special pair (P, red), accessory bacteriochlorophylls (B_L, yellow; B_M, orange), bacteriopheophytins (H_L, blue; H_M, purple), quinones (Q_A, light green; Q_B, green), nonheme iron (Fe, dark red), and carotenoid (crt, cyan). The L subunit is in tan, and the M subunit is in gray.

As also seen in Figure 1, an alternative M-side pathway of chemically identical electron acceptors, denoted B_M and H_M, is available. However, ET to H_M in native RCs is slow (~100 ps) relative to ET to H_L,[5,6] which is why this process is typically not observed. A handful of mutants have elicited ET from P* to H_M,[4,5,7−11] with the shortest time constant observed to date ~40 ps.[8] P* decay in these mutants sometimes has been found to be nonexponential with differing photochemistry in populations of RCs that are not interconverting on the picosecond time scale; the populations differ in the relative amounts of ET to the L-side versus the M-side versus nonradiative decay to the ground state.[4,11−13] For example, in two D_{LL}-based mutants where we trapped $P^+B_L^-$, near quantitative yield of this state was obtained in an ~50% P* population having a 5−10 ps lifetime; however, the other ~50% P* population had an ~100 ps lifetime and decayed via ET to H_M and ground state recovery.[4] Thus, even though ET from P* to B_L occurred in ≤10 ps in one subpopulation, it appeared to be suppressed in the other.

The origin of this paradoxical result is not known; however, we were led to speculate that it might involve the Tyr residue at

Received: May 30, 2012
Revised: July 15, 2012
Published: August 9, 2012

   dx.doi.org/10.1021/jp305276m | *J. Phys. Chem. B* 2012, 116, 9971−9982

position M208. Figure 2 shows a close-up view of the B_L environment. (Note that the present work utilizes *Rb. capsulatus* RCs; in *Rb. sphaeroides* the equivalent position is M210.) This Tyr is unusual in that it is the only Tyr (out of 28 in *Rb. sphaeroides*) that appears in the highest resolution X-ray structure (2j8c in the Protein Data Bank[14]) to lack a hydrogen bond partner to its phenolic −OH group. An X-ray structure of the *Rb. capsulatus* RC has not been reported but is expected to be very similar to *Rb. sphaeroides*; there are 33 tyrosines in *Rb. capsulatus*. This was confirmed by observing the solid state ^{13}C NMR spectrum in *Rb. sphaeroides* RCs where all tyrosines are labeled at the carbon adjacent to the hydroxyl group, whose chemical shift is very sensitive to hydrogen bonding; the Tyr at M210 was specifically assigned by mutagenesis.[15] (This measurement has been repeated for *Rb. capsulatus* RCs and identical behavior observed; Carter, B.; Saggu, M.; Zhou, X.; Cegelski, L.; Holten, D.; Boxer, S. G.; Kirmaier, C. unpublished results.) The importance of this Tyr has been widely investigated by mutagenesis[16−18] and by simulations.[19] Replacement of Tyr by other amino acids generally slows ET to the L-side but does not prevent it. Molecular dynamics simulations suggest that the two most populated orientations of the Tyr hydroxyl, involving rotation around the −OH bond (in each orientation the −OH is roughly in the plane of the aromatic ring), position the −OH dipole quite differently relatively to B_L, in one orientation stabilizing $P^+B_L^-$, while in the other orientation destabilizing $P^+B_L^-$.[20,21] A possible origin of the (nominally) two populations described above in two D_{LL}-based mutants that both have a Tyr at M208 is that in one population $P^+B_L^-$ forms because the tyrosine −OH is in the stabilizing position, whereas in the other population the −OH

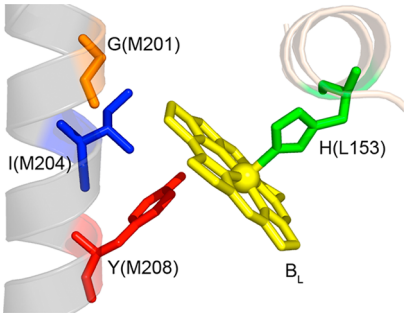

Figure 2. Protein environment around B_L (from the *Rb. sphaeroides* crystal structure[14])with key residues labeled. For clarity only the D helix of the M subunit and the interhelix region of the L subunit are shown.

Table 1. Mutants Used in This Work[a]

Mutant	Mutations	General Effects of Mutations	Chromophore diagram	Pigment Ratio BChl:BPh	P/P$^+$ midpoint potential (mV)
WT	none	not applicable	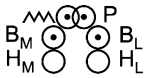	1.91 (±0.04)	500
Q	I(M204)Q	B_L-less	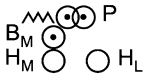	1.52 (±0.07)	452
QH	I(M204)Q/L(M212)H	B_L-less, BChl in the H_L site	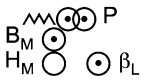	3.27 (±0.04)	-
LQ	G(M70)L/I(M204)Q	B_L-less, carotenoid-less	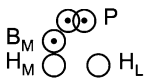	1.48 (±0.19)	-
DQ	V(M131)D/I(M204)Q	B_L-less, red shifted H_M Q_x band		1.46 (±0.09)	-
YQ	F(L181)Y/I(M204)Q	B_L-less, stabilizing Tyr near B_M		1.49 (±0.16)	439
YQH	F(L181)Y/I(M204)Q/ L(M212)H	B_L-less, stabilizing Tyr near B_M, BChl in the H_L site	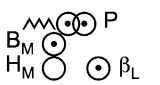	3.03 (±0.02)	437
YLQ	F(L181)Y/G(M70)L/ I(M204)Q	B_L-less, stabilizing Tyr near B_M, carotenoid-less	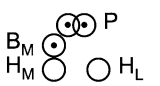	1.32 (±0.10)	-
ΦQ	H(M180)L/I(M204)Q	B_L-less, BPh in the B_M site	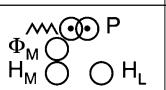	0.56 n/a	-

[a]The first and fourth columns contain the shorthand name and chromophore diagram, respectively, corresponding to the absorption spectra in Figure 3. In the chromophore diagrams, circles with dots represent BChls, open circles represent BPh, and the sawtooth line represents the carotenoid.

dx.doi.org/10.1021/jp305276m | J. Phys. Chem. B 2012, 116, 9971−9982

is in the destabilizing orientation disfavoring ET to B_L. Although entirely speculative, this led us to consider whether it might be possible to introduce a hydrogen bond to the Y(M208) hydroxyl group and pin down its orientation.

Examination of the key amino acids near Y(M208) led us to the isoleucine at M204 (Figure 2) as a residue that could be mutated to one that might hydrogen bond with the hydroxyl group of the Tyr at M208, enforcing a specific orientation. Based on simple modeling, two possibilities emerged, replacement with glutamine, I(M204)Q, or with glutamic acid, I(M204)E, and both variants were prepared. As described in detail in the following, we were very surprised to discover that the I(M204)Q mutant appears to assemble without any chromophore in the B_L binding site. This provides a simple method, based on a single amino acid change, for entirely shutting down ET to the L-side and affords an ideal platform for studying ET along the normally nonfunctional M-side. A series of further mutations in the I(M204)Q background are also described here to clarify spectral assignments and enhance ET to the M-side. Interestingly, the I(M204)E variant does assemble with a BChl in the B_L binding site; however, its photochemistry is quite different from WT and from the I(M204)Q mutants reported here. Additionally, there is evidence that Y(M208) is now hydrogen bonded in I(M204)E (Carter, B.; Saggu, M.; Zhou, X.; Cegelski, L.; Holten, D.; Boxer, S. G.; Kirmaier, C. unpublished results). These results will be presented in a separate paper.

EXPERIMENTAL SECTION

Mutagenesis and RC Expression. Site-directed mutagenesis of all *Rb. capsulatus* strains and RC expression and purification were carried out largely as described previously.[22] Following batch binding of the His-tagged RC to Ni-NTA agarose resin that was pre-equilibrated with 10 mM Tris (pH 8.0), 0.05% Deriphat 160-C, 300 mM NaCl, and 5 mM imidazole buffer, the resin was collected in a column and washed with 200 mL of the equilibration buffer. RCs were eluted with buffer containing 10 mM Tris (pH 8.0), 0.1% Deriphat 160-C, 300 mM NaCl, and 300 mM imidazole.

It was found that all RCs containing the I(M204)Q mutation had a large proportion of P-less RCs, which could be separated by anion exchange chromatography using three Q Sepharose HP HiTrap columns (GE Healthcare) in series with a sufficiently shallow gradient in [NaCl] (0.5 mM NaCl/mL at a flow rate of 10 mL/min). Putting the P-less fraction under reducing conditions did not restore the 850 nm Q_Y absorption band of P, so this is not a population wherein P had become oxidized to P^+. In the P-containing fraction, after many hours of storage in the dark at room temperature, the Q_Y band of P decreased and a new P-less fraction could be separated using the above-described method; consequently once isolated RCs were kept on ice while in use and at −80 °C long-term. The first four columns of Table 1 summarize the eight mutants prepared, their shorthand codes and other key characteristics, with the results of pigment extractions and P redox measurements collected in the last two columns. All measurements were made on the P-containing fractions in 10 mM Tris (pH 8.0) buffer containing 0.05% Deriphat 160-C and 300 mM NaCl, unless otherwise noted.

Characterization Methods. Low-temperature absorption spectra of RCs in 50% glycerol (v/v) were acquired using a liquid nitrogen immersion cryostat.[23] Pigment extractions in 7:2 acetone/methanol were performed as per van der Rest and Gringas;[24] for each mutant, at least three extractions trials were performed except where noted. The midpoint potentials of RCs were determined by chemical titration of the Q_Y absorption band of P with additions of potassium ferro- and ferricyanide. A 1000-fold molar excess of ferrocyanide relative to the [RC] was first added to ensure that P was fully reduced. Then, additions of ferricyanide were made to increase the potential at which the solution was poised. The potential was monitored with a Pt wire versus a Ag/AgCl microelectrode (Edaq) reference that was calibrated before each use with ferricyanide/ferrocyanide solutions. Measurements were corrected for Ag/AgCl versus NHE (220 mV). The data were well fit by a one-electron Nernst equation. Picosecond transient absorption (TA) measurements utilized ∼130 fs excitation flashes at either 855 or 590 nm. RC samples were held at 10 °C in a small reservoir and flowed through a 2 mm path length cell. Other details were as previously described.[8]

RESULTS AND DISCUSSION

RCs with I(M204)Q are B_L-Less. The ground state absorption spectrum of I(M204)Q shows a striking reduction in the band at ∼800 nm, assigned as the Q_Y band of the BChls in the B-sites, compared to WT (Figure 3). The peak maximum of this band in I(M204)Q red shifts 9 nm relative to WT. Based on previous assignments,[25,26] the BChl in the B_L site contributes to the blue side of this band and B_M to the red

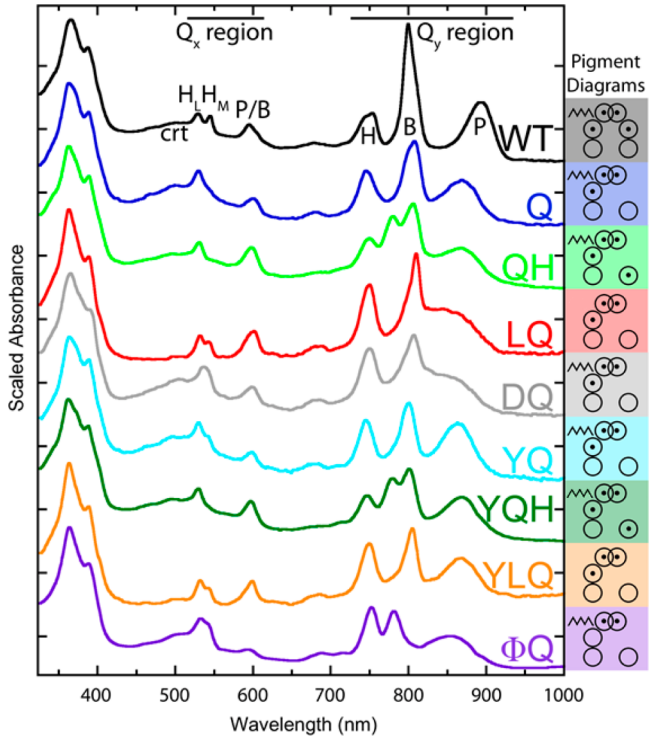

Figure 3. Absorbance spectra at 77 K of WT and mutants used in this study. The pigment diagrams on the right indicate the presumed chromophore arrangement in each mutant. Circles with dots represent BChl, open circles represent BPh, and sawtooth lines represent carotenoid. Overlapped circles at the top of each diagram represent the P chromophores, circles in the middle represent the chromophores in the B sites, and circles at the bottom represent the chromophores in the H sites. Dots in the circles represent the central Mg ion of a BChl. The L-side chromophores are on the right, and M-side chromophores are on the left.

dx.doi.org/10.1021/jp305276m | J. Phys. Chem. B 2012, 116, 9971−9982

side; thus the loss of B_L would be expected to result in a reduction of the intensity of the band by roughly half and a red shifting of the peak. Note also that the Q_Y band of P shifts considerably to the blue, presumably reflecting the loss in the interaction between P and B_L, and this shift also contributes to the red shift of the band at 800 nm since the two bands overlap. Similarly, changes in the Q_Y absorption band of H_L near 760 nm could reflect loss of interactions with B_L.

As shown in Table 1, the BChl/BPh ratio of I(M204)Q was found to be 1.52, which can only be reasonably reached (and remain consistent with the absorption spectrum) by the removal of one BChl from the WT chromophore composition leaving three BChl and two BPh. A similar ratio is found for the four other mutants expected to have the same bacteriochlorin composition as I(M204)Q (variants YQ, DQ, LQ, and YLQ in Table 1). In the following, we will often refer to any variant missing a chromophore in the B_L binding site as "B_L-less" for simplicity.

RC Variants in the I(M204)Q Background. Variants of I(M204)Q containing key mutation(s) that have been characterized in detail in other contexts were made to provide additional evidence for the loss of BChl from the B_L site, to assist in the assignment of ground-state and TA spectra or to enhance M-side ET. In the H(M180)L/I(M204)Q mutant (denoted ΦQ, Table 1), the axial His ligand of B_M at M180 is replaced with a noncoordinating Leu and results in replacement of the BChl with a BPh (Φ_M) in the B_M site.[27−29] Compared to WT, the UV−vis spectrum of ΦQ shows a complete absence of an 800 nm absorption band and a new band at 781 nm, indicative of a loss of both BChls in the B-sites and the incorporation of a new BPh (Figure 3). Katilius et al. reported a similar Q_Y band of Φ_M at ∼785 nm in the H(M182)L mutant of *Rb. sphaeroides*.[27] These spectral data and the pigment composition of 0.56 BChl/BPh are consistent with an RC in which one BChl is replaced with BPh and a second BChl is removed entirely, thus supporting the conclusion that the I(M204)Q mutation results in B_L-less RCs. Several of the BChl:BPh ratios in Table 1, including for ΦQ, are lower than expected and will be discussed further below.

Characteristic Q_X absorptions for the H_L and H_M BPhs are found near 529 and 544 nm, respectively, in the ground state absorption of WT at low temperature (Figure 3, top). As seen in Figure 3, these absorption bands are not resolved at low temperature in I(M204)Q. Since these bands are critical for distinguishing whether ET proceeds down the L- and/or M-branch, variants I(M204)Q/L(M212)H and V(M131)D/I(M204)Q (denoted QH and DQ,) were made to alter the spectral properties of H_L and H_M, respectively. The mutation L(M212)H causes a BChl (denoted β_L) to bind in place of BPh in the H_L binding pocket by providing an axial ligand for the central Mg^{2+}.[30] This shifts the Q_X absorption of the chromophore in the H_L site (now a BChl) to around 600 nm, and as the only remaining BPh, the BPh in the H_M site is the only bacteriochlorin absorbing around 529 nm. As seen in Figure 3, the ground state absorption spectrum of QH (and also YQH, see below) is consistent with the replacement of a BPh with a BChl, as typified by the spectral changes seen in L(M212)H versus WT.[30] Variant V(M131)D/I(M204)Q (denoted DQ) was made to alter the spectral properties of H_M, again to facilitate specific assignment of ET to H_M by TA measurements. The V(M131)D mutation creates a hydrogen bond to the ring V keto group of H_M, and red shifts its Q_X absorption by 3−4 nm in comparison to WT.[31,32] In the DQ spectrum (Figure 3), a small red shift of the Q_X absorption envelope is noted.

Another strategy to better resolve the H_L and H_M Q_X absorption bands relied on removal of the carotenoid, which has broad and somewhat structured absorption between ∼450 and ∼550 nm. Carotenoidless mutants were created using the mutation G(M70)L.[33] In the spectra (Figure 3) of both G(M70)L/I(M204)Q and F(L181)Y/G(M70)L/I(M204)Q (denoted LQ and YLQ, respectively), the "baseline" in the 450−550 nm region is much flatter, consistent with loss of the carotenoid. It can be seen in the low temperature spectrum that the Q_X absorption bands of H_M and H_L are resolved as peaks at 532 nm and a shoulder at 542 nm, respectively, suggesting that the I(M204)Q mutation does not abolish distinction between the Q_X absorption bands of H_L and H_M.

Finally, the YQ, YQH, and YLQ variants were made in which a Tyr replaces the native Phe at L181, the symmetry-related position to M208 (Figure 2). L181 is in close proximity to B_M and a Tyr at this position has been shown to promote M-side ET.[8−10] Thus, F(L181)Y was combined with the Q and QH and LQ variants to examine the effect on the rate and yield of ET to the M-side.

The BChl:BPh ratios found by pigment extraction for QH (3.27) and YQH (3.03) are ∼20% below the expected value of 4:1 for RCs that are B_L-less and have a BChl in the H_L site (Table 1). Most of the pigment extractions gave BChl/BPh ratios lower than expected, with the non β-containing RCs averaging about 10% low. It can only be speculated as to whether there is possibly incomplete extraction of the BChl chromophores or incidental demetalation of BChl to BPh, both of which would give rise to a lower BChl/BPh ratio. We also note that low BChl/BPh ratios (usually low by 5−10%) are typically reported for the RC pigment extraction method used here.[28,30,34]

Mutation at the C_2-Symmetry Related Position L177 and Other Constructs. Introducing Gln at L177, the symmetry-related position to M204, did not result in the absence of a pigment in the B_M site as assayed by the UV−vis spectrum of I(L177)Q, which is nearly identical to that of WT (data not shown). This suggests that unique environmental elements of the B_L site work in conjunction with the introduced Gln at M204 to knock the BChl out of the B_L binding site. A similar selective effect was seen for the H_L and H_M knockout mutants, where the symmetry-related mutations failed to knock out the corresponding chromophores.[3,35]

It is fair to say that in most cases the mechanism(s) that lead to chromophore exclusion and relative stability of the resulting RCs are not clear. Typical expression yields (defined as the amount of protein isolated from a liquid culture of bacteria) for WT are 7−10 mg RC/L culture media using the expression and isolation protocols described above, and the expression yield of the I(M204)Q B_L-less mutant is comparable. Many of the other mutants reported here had somewhat lower (at most a factor of 4) but practicable yields. Two other constructs we made gave no or very poor RC yields: (1) I(M204)Q added to the D_{LL} background[3] resulted no RCs and (2) I(M204)Q added to A(M147)W,[35] which by itself knocks out H_M, gave a very poor expression yield of ∼0.03 mg RC/L culture media. There is ample evidence to show that the RC protein can accommodate many and varied mutations while still folding into a native-like structure. However, the loss of both a BChl and BPh seems to result in unstable RCs as observed by the low expression yields of these two mutants.

dx.doi.org/10.1021/jp305276m | J. Phys. Chem. B 2012, 116, 9971−9982

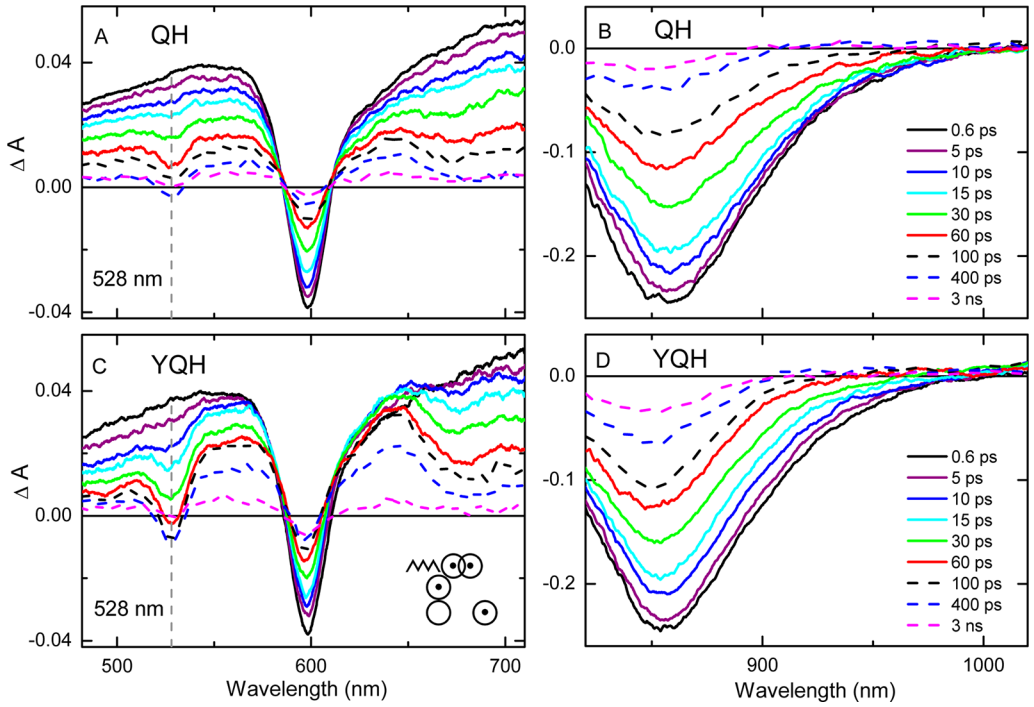

Figure 4. Transient absorption spectra of QH and YQH at 295 K acquired after a 130 fs excitation flash at 850 nm (panels A and C) or 600 nm (panels B and D). The chromophore diagram for QH and YQH (shown in panel C) is described in Figure 3.

Recently, a B_L-less RC has been proposed by Leonova et al. in a mutant that replaces the axial ligand to B_L, H(L153), with Tyr.[36] RCs could not be isolated, so evidence for a B_L-less RC came from examination of room temperature absorbance spectra, photoinhibition of respiration action spectra, and pigment extraction, all of which were performed on RCs in chromatophores. This same mutant had been made previously by Katilius et al., who found that RCs isolated in LDAO or Trition X-100 contained a P-less fraction that could be separated out.[28] In that work it was concluded that the pigment composition of the P-containing fraction was unchanged from that of WT. It should be noted that BChl/BPh ratios from pigment extractions that include P-less RCs, which cannot be separated away in a chromatophore preparation, will be skewed to a lower value. The discrepancy regarding the pigment content of H(L153)Y remains unresolved.

P Redox Potential Measurements. The P/P^+ midpoint potential of I(M204)Q is ~50 mV below the WT value of +500 mV versus NHE (Table 1). In the YQ and YQH variants, the P/P^+ midpoint potential is lowered further with the additional decrease attributed to the F(L181)Y mutation. An ~25 mV lowering of the P/P^+ midpoint potential in the single F(L181)Y mutant was reported previously.[37] Individual mutations are not expected to have a perfectly additive effect on the P/P^+ potential; the small deviation from additivity observed here is similar to that seen in other series of mutations designed to modify the P/P^+ potential.[38,39]

Picosecond Measurements of Electron Transfer to H_M in the I(M204)Q Mutants. The major focus of this section is to describe the evidence for ET to the M-side BPh (H_M) in the I(M204)Q mutants, and complete lack of evidence for ET to H_L. To positively identify the direction of ET in the I(M204)Q-containing mutants, these studies focused on the variants that were designed to alter the absorption properties of the pigment in the H_L site by replacement with the β_L cofactor or alter the absorption properties of H_M (e.g., hydrogen bond to H_M via the V(M131)D mutation).

Picosecond TA spectra in the visible and near-IR regions for the β_L-containing QH and YQH mutants are shown in Figure 4. At the earliest times (0.6 ps, Figure 4, panels A and C), the TA spectra are assigned to P*, which has a broad, mostly featureless absorption between 480 and 700 nm and bleaching of the Q_X ground-state absorption band of P at 598 nm. In the Q_Y region (Figure 4, panels B and D), bleaching of the long-wavelength ground state absorption band of P at ~855 nm is observed along with stimulated emission from P* extending to ~1000 nm on the long-wavelength side of the P bleaching. The spectra at later times show that stimulated emission from P* persists to ≥100 ps after excitation (Figure 4, panels B and D), indicating a long P* lifetime. It is also clear from cursory examination of the data in Figure 4, panels B and D, that the majority P* decay pathway is P* → P, as indicated by the large decay of P bleaching, evident in the 830−850 nm region where stimulated emission does not contribute, and also in the Q_X band of P at 598 nm (Figure 4, panels A and C). The main features of the picosecond TA spectra of the other five mutants examined (Q, YQ, LQ, YLQ, and DQ) are essentially identical to those shown in Figure 4. (Picosecond measurements were not performed on the ΦQ mutant due to low RC yields.) All seven RCs exhibit dual P* stimulated-emission decay components: (1) a shorter component of either ~20 ps (when there is a Tyr at L181) or ~40 ps (when there is the native Phe at L181) and (2) a longer component of ~130 ps. Analysis and interpretation of the complex P* decay is presented in the following section.

Evidence that ET from P* to H_M occurs is seen in the TA spectra shown in panels A and C of Figure 4. By about 100 ps bleaching at 528 nm and an absorption band near 640 nm have developed to near maximal amplitude in both QH and YQH.

dx.doi.org/10.1021/jp305276m | J. Phys. Chem. B 2012, 116, 9971−9982

These spectral features are the signatures of the charge-separated state $P^+H_M^-$,[5,7,8,10] and are a straightforward assignment in the QH and YQH mutants where a BChl (β_L) replaces H_L. The L(M212)H mutation has been used extensively to unambiguously resolve ET to H_M.[5,7−9] Here the motivation was even greater in light of the poor distinction between the Q_X bands of H_L and H_M even at low temperature in the I(M204)Q mutants. A quantitative comparison of the $P^+H_M^-$ spectra and yield of this state among the seven mutants is presented in Figure 5. Obtained under near identical

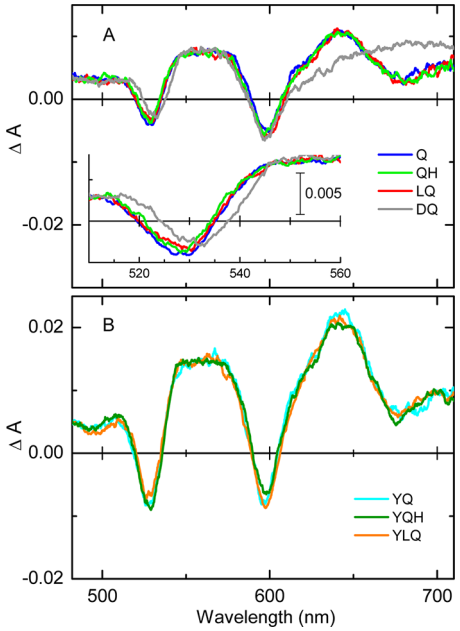

Figure 5. Comparison of the Q_X and anion region transient absorption spectra for Q, QH, LQ, and DQ (A) and YQ, YQH, and YLQ (B) at ∼400 ps. Spectra were acquired using 130 fs excitation flashes at 850 nm and have been normalized to the same initial P* concentration.

experimental conditions, the spectra in Figure 5 have been normalized by factors of 1 to 1.2 (to adjust for slight differences in sample concentration and/or laser excitation conditions), so that they have an identical magnitude of P bleaching at ∼598 nm at 0.6 ps. The spectra shown in Figure 5 were taken at ∼400 ps (ranging from 380 to 450 ps) by which time the contribution of the long-lived P* species to the TA difference spectra is minimal.

The spectra for Q, QH, and LQ have essentially identical magnitudes and positions of BPh Q_X ground state bleaching at 528 nm and BPh anion absorbance at 640 nm (Figure 5A). Spectra essentially identical to each other are also obtained for YQ, YQH, and YLQ (Figure 5B). Collectively, the spectra show that identical BPh-associated features are obtained following completion of P* decay whether the RC contains the native BPh, H_L, (in Q, LQ, YQ, and YLQ) or has instead a BChl, β_L, (in QH and YQH). Thus, the charge-separated state resulting from P* decay can be assigned with confidence to $P^+H_M^-$. Note further that the absolute magnitudes of the $P^+H_M^-$ spectra are roughly 2-fold greater for YQ, YQH, and YLQ compared to Q, QH, and LQ. Thus, the yield of $P^+H_M^-$ is roughly 2-fold greater for the RCs that contain Tyr at L181 compared to the ones that contain the native Phe.

Additional support for formation of $P^+H_M^-$ is obtained from the distinguishing characteristics of the TA spectrum of DQ in Figure 5A. As described above, the Asp at M131 in the DQ mutant was designed to red shift the Q_X band of H_M by addition of a hydrogen bond. The 531-nm ground state absorbance (Figure 3) and bleaching in the TA data (Figure 5) are in concert and thus support ET to H_M. The magnitude of BPh Q_X bleaching in DQ matches very well with the magnitudes of bleaching at 528 nm in Q, QH, and LQ. Note also that the well-resolved BPh anion band at ∼640 nm in the other mutants is replaced in DQ with a red-shifted, weaker and broader absorption. These results are identical to ones previously reported for the V(M131)D mutation in another set of background mutations that provide M-side ET.[32] Thus, the distinguishing features of the picosecond TA spectra of DQ directly support the formation of $P^+H_M^-$ (as opposed to $P^+H_L^-$) in this mutant.

Further evidence that supports formation of $P^+H_M^-$ in all seven RCs is that the spectral features of this state persist, but have partially decayed on the ∼3 ns time scale of the measurements. This can be seen in Figure 4, where bleaching at 528, 600, and 850 nm and the BPh anion absorption band at 640 nm are reduced in magnitude but still present at 3 ns. This finding is consistent with the known 1.7 or 3.2 ns lifetime of $P^+H_M^-$ depending on whether Q_B is fully occupied or absent/blocked, respectively.[40]

We conclude this section with a determination of the yield of $P^+H_M^-$ in the seven mutants studied based on the spectra in Figures 4 and 5. The overall yield of $P^+H_M^-$ is obtained by taking the ratio between the amount of $P^+H_M^-$ formed (given by the maximal magnitude of 528-nm bleaching attained) and the initial amount of P* formed (given by the magnitude of P bleaching at 598 nm at 0.6 ps). It is assumed that the extinction coefficient of H_M at 528 nm is approximately equal to that of P at 598 nm, as is the case for the 542 nm Q_X absorption of H_L. This assumption has been adopted in previous cases where the yield of ET to H_M has been determined and was validated in a mutant in which $P^+H_M^-$ is the sole charge-separated product of P* decay and forms in very high (70%) yield.[10] The yields of $P^+H_M^-$ determined in this manner (method 1) are collected in column 2 of Table 2. The consistency among Q, QH, LQ, and DQ and among YQ, YQH and YLQ is clear with average observed yields of $P^+H_M^-$ of 18% and 35% for the two groups, respectively. Thus, the yield of $P^+H_M^-$ is about a factor of 2

Table 2. Observed Yield of $P^+H_M^-$ in M204Q Variants[a]

RC	method 1[b]	method 2[c]	method 3[d]
Q	23%	21%	22%
QH	14%	16%	16%
LQ	18%	n.d.	n.d.
DQ	16%	n.d.	n.d.
YQ	40%	32%	42%
YQH	35%	31%	35%
YLQ	32%	n.d.	n.d.

[a]n.d. = insufficient data to perform the analysis due to sample decomposition. [b]Method 1: Derived from comparison of the maximal H_M bleaching at 528 nm to the initial amplitude of P bleaching at 598 nm at 0.6 ps. The experimentally observed maximal H_M bleaching is attained at ∼150 ps in Q, QH, LQ, and DQ and at ∼80 ps in YQ, YQH, and YLQ. [c]Method 2: Determined from the amplitude (a fit parameter) of the 1.7 ns component of decay of P bleaching at 840−850 nm compared to the total amplitude. [d]Method 3: Determined from the amplitude (a fit parameter) of the 1.7 ns component of decay of P bleaching at 594−602 nm compared to the total amplitude.

dx.doi.org/10.1021/jp305276m | J. Phys. Chem. B 2012, 116, 9971−9982

higher when there is a Tyr at L181 rather than the native Phe. The yields determined here (method 1) come from spectral analysis: a comparison of the Q_X bleaching magnitudes of H_M and P. They are in excellent agreement with the values for the $P^+H_M^-$ yields presented in columns 3 and 4 of Table 2, which utilize methods that are derived from the relative amplitudes of the fit components of the P* decay kinetics, as will be described in the following section.

General Model for P* Decay Pathways. This section lays out a general model given in Figure 6 that is consistent with the complex kinetics observed in all seven of the I(M204)Q mutants studied; Figure 6 give specific results for four of the mutants. The general model is characterized by two different populations of P* that are in roughly 70:30 proportion (varying from ~60:40 to ~80:20 between samples and data sets). These P* populations are distinguished by having different P* lifetimes and different decay pathways, the specific details of which will be developed in this and the following sections. Four mutants for which the highest quality and largest amount of data were collected—Q, QH, YQ, and YQH—contributed most to development of the model. Sufficient data were obtained for the other three mutants to determine that the P* decay kinetics and yield of $P^+H_M^-$ in LQ and DQ are similar to those found in Q and QH, and analogously YLQ is similar to YQ and YQH.

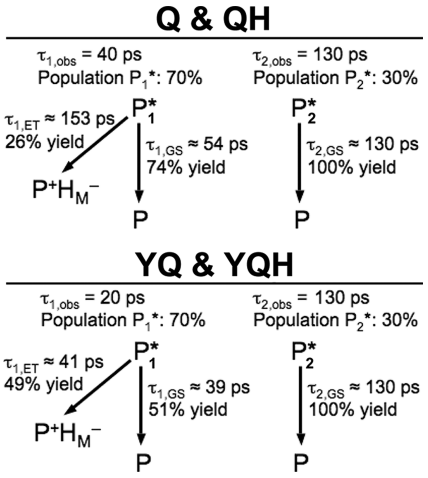

Figure 6. Proposed working model involving two photochemically distinct subpopulations in I(M204)Q-containing mutant RCs. The observed time constants are indicated above each scheme, along with the relative proportion of RCs that follow each scheme. The calculated time constant and yield of the associated process is given next to the arrows indicating the P* decay pathways. See text for further details.

Figure 7B shows the P* stimulated emission decay profile for QH (averaged data between 900 and 910 nm) and fits to one- and two-exponential functions. This wavelength range spans a near isosbestic point in the $P-P^+Q^-$ difference spectrum, $\Delta A \approx 0$ at ~905 nm; therefore, little if any P-bleaching or P^+ absorption contributes to the absorption changes over this wavelength range. The data are better fit by the two-exponential than the one-exponential function. The time constants and relative amplitudes returned by the two-exponential fit are 41 ± 6 ps (66%) and 136 ± 32 ps (34%).

Similar results are obtained from the fit of the P-bleaching decay kinetics at 840–850 nm, near the peak of the ground-state Q_Y band of P band (Figure 7A). It can be seen that the time profile in this region is better fit with three exponentials than two exponentials functions, both cases utilizing a fixed 1.7 ns component for the (known) $P^+H_M^-$ lifetime[40] (whose amplitude was a free fitting parameter). The values and relative amplitudes of the two fit time constants are 32 ± 4 ps (66%) and 152 ± 30 ps (34%), all of which are in good agreement with the values determined from the P* stimulated-emission decay kinetics. The 840–850 nm bleaching data and fit also provide a measure of the yield of $P^+H_M^-$ (method 2), which is given by the fit amplitude of the fixed 1.7-ns time constant relative to the amplitude of total bleaching. The $P^+H_M^-$ yield so determined is 16% for QH (method 2 in column 3 of Table 2). The decay of bleaching of the Q_X band of P at 594–602 nm (data not shown) were similarly better fit using a three- versus two-exponential function, where one time constant is fixed at 1.7 ns for the $P^+H_M^-$ lifetime. The time constants for P* decay obtained from the three-exponential fit are 28 ± 6 ps and 98 ± 13 ps. The amplitude of the 1.7-ns decay component gives a 16% yield of $P^+H_M^-$ (method 3 in column 4 of Table 2). There is good agreement in Table 2 between the yields of $P^+H_M^-$ determined for QH by all three methods.

Unlike the kinetics associated with overall P* decay, the appearance and decay of bleaching of the Q_X band of H_M at 528 nm is well fit by a simple two-exponential function (Figure 8A), where decay of H_M bleaching at 528 nm (the $P^+H_M^-$ lifetime) is fixed at 1.7 ns. This fit returns a value for the appearance of H_M bleaching (and per force the lifetime of the parent P* state) of 37 ± 4 ps. This time constant is in excellent agreement with the faster component of the P* decay obtained above in the other spectral regions. Attempts to fit the time profile at 528 nm shown in Figure 8A with three exponentials showed that there is at most a few percent contribution from the 130 ps P* decay component found in other spectral regions discussed above. Therefore, the P* population (35% amplitude) that decays with an ~130 ps time constant is not associated with $P^+H_M^-$ formation, instead decaying only via P* → ground state. It is in the P* population (65% amplitude) having an ~40 ps lifetime that ET to H_M takes place. Additionally, since the ~40 ps component is observed in the P bleaching decay kinetics (840–850 nm and 590–600 nm), this population of P* also decays in some part via ground state recovery.

This survey of the time evolution of the absorbance changes in key wavelength regions for QH RCs provides a consistent set of results that is reflected in the generalized schemes in Figure 6. Similar results are obtained for the Q mutant (data not shown, but see, e.g., the $P^+H_M^-$ yields determined via methods 2 and 3 in Table 2). Data analysis for YQ and YQH revealed an essentially identical overall pattern of results, but with the important differences that P* → $P^+H_M^-$ charge separation is faster and the yield of $P^+H_M^-$ is about 2-fold larger as compared to Q and QH. Representative data for YQH are shown in Figure 7, panels C and D. The time constants and relative amplitudes for P* stimulated-emission decay in YQH (Figure 7D) are 21 ± 3 ps (70%) and 97 ± 22 ps (30%), with similar time constants and relative amplitudes for P* decay obtained from analysis of the 840–850 nm data (Figure 7C) and 594–602 nm data (not shown). Once again a critical finding is that the bleaching at 528 nm develops with a time constant of 19 ± 2 ps, a value that matches the faster component of both P* stimulated emission decay and P-bleaching decay (Figure 8B). The yields of $P^+H_M^-$ determined from the fits of the Q_Y and Q_X P-bleaching decay in YQ and YQH are given in Table 2. The respective yields agree well with the values determined from

dx.doi.org/10.1021/jp305276m | J. Phys. Chem. B 2012, 116, 9971–9982

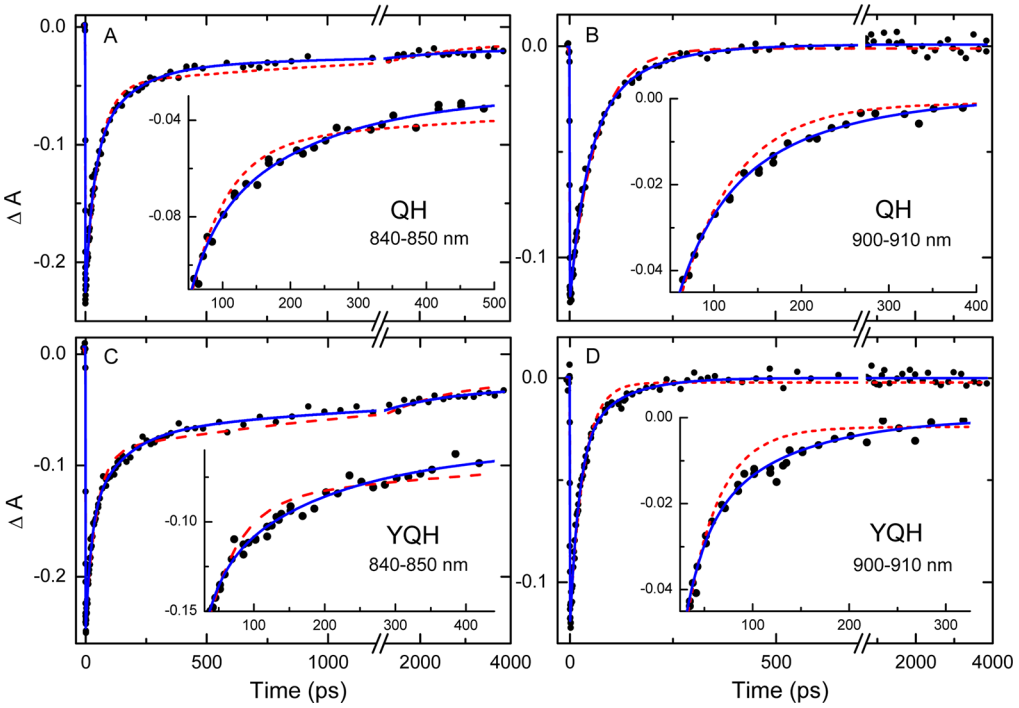

Figure 7. Kinetic data and fits for QH RCs (A and B) and YQH RCs (C and D) at 295 K. Parts B and D show decay of P* stimulated emission averaged between 900 and 910 nm (●) and fit to the instrument response plus a single exponential plus a constant (red, dashed) and fit to the instrument response plus two exponentials plus a constant (blue, solid). Parts A and C show decay P bleaching averaged between 840 and 850 nm (●) and fit to the instrument response plus two exponentials plus a constant with one exponential held fixed at 1.7 ns (red, dashed) and fit to the instrument response plus three exponentials plus a constant with one exponential held fixed at 1.7 ns (blue, solid). See text for further details. The insets examine sections of the plots drawing attention to distinctions between the data and fitting results.

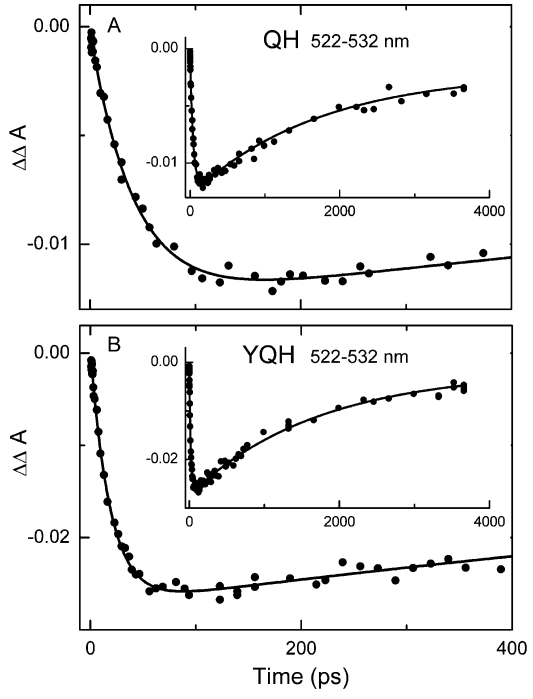

Figure 8. Representative kinetic data (●) and fits (solid lines) for the appearance and decay of bleaching of the Q_X band of H_M averaged between 522 and 532 nm for QH RCs (A) and YQH RCs (B) at 295 K, referenced to absorption changes (averaged) between 550 and 565 nm. In both panels the fit is to a dual exponential for the appearance (fit parameter) and decay (1.7 ns fixed component) of H_M bleaching.

method 1 and are consistently close to a factor of 2 higher than those determined for Q and QH.

Global Analysis via SVD. The entire 500−700 and 830−1000 nm ranges of TA data (spanning before zero-time to ∼4 ns) for each of Q, QH, YQ, and YQH were subject to principal-component analysis by singular value decomposition (SVD) followed by global analysis to obtain species-associated spectra of the components described above. As for the individual wavelength data analyses presented above, global fitting required two fit exponentials plus a fixed 1.7-ns exponential (for decay of $P^+H_M^-$). The global analysis for YQH returned time constants of 20 and 130 ps. Figure 9, panels A and B, shows the decay-associated spectra (spectra of the exponential prefactors) for the 20 ps, 130 ps, 1.7 ns, and asymptotic (long time) components. The 20 ps Q_x region decay-associated spectrum has key features at 528 and 640 nm connected with H_M reduction; however, such features are clearly absent in the 130 ps decay-associated spectrum. Figure 9, panels A and B, clearly shows that both the 20 and 130 ps decay-associated spectra display features attributable to P* stimulated emission (900−100 nm) and P bleaching (at 600 and 850 nm). The species-associated spectra (spectra of the intermediates) in Figure 9, panels C and D, derive from application of the general model in Figure 6. The spectral features of the 20-ps and 130-ps species are both appropriate for P* and the 1.7 ns and long-lived species consistent with $P^+H_M^-$ and $P^+Q_B^-$, respectively. The features in both the decay- and species-associated spectra reveal, as expected based on the wavelength-by-wavelength analysis given above, that the 130 ps P* population decays exclusively to the ground state and the 20 ps P* population alone affords ET to H_M, along with competing repopulation of the ground state.

dx.doi.org/10.1021/jp305276m | J. Phys. Chem. B 2012, 116, 9971−9982

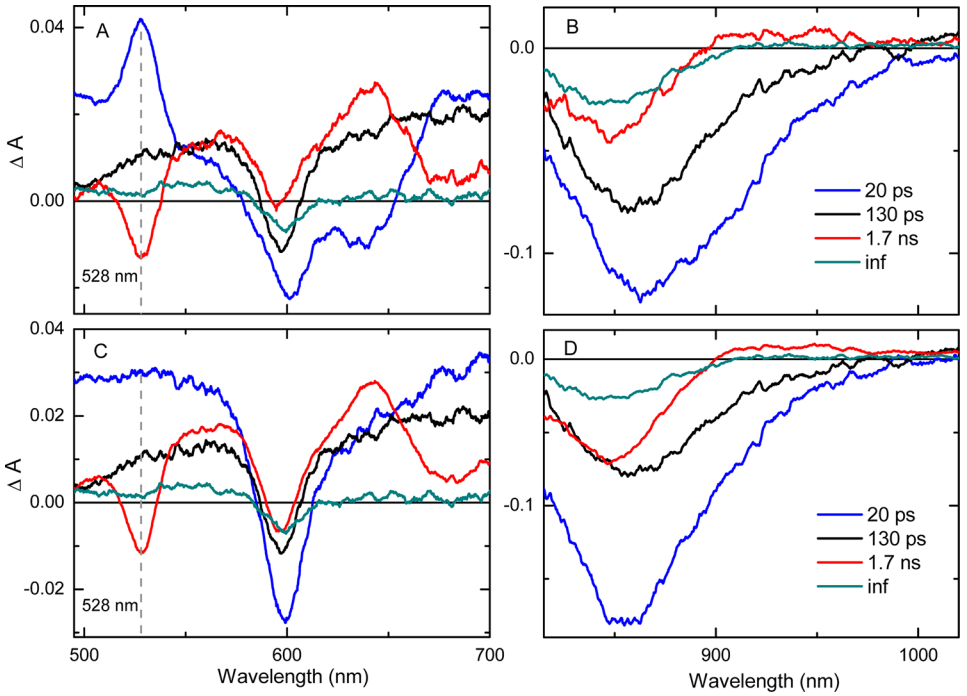

Figure 9. Decay associated (amplitude) spectra in the visible (A) and near-infrared (B) regions for YQH RCs resulting from SVD and global analysis, and the corresponding species-associated spectra (C and D) resulting from application of the model given in Figure 6. The black spectrum is identified as a P* fraction that decays only to the ground state. See text for details.

Summary of the Photochemistry in the Two P* populations. Summary values for the unique decay pathways within the two P* populations are given in the schemes in Figure 6 and derived as follows. The amplitude ratios of the two P* decay components (shorter-lived P_1* and longer-lived P_2*) vary from 64%/36% to 78%/22% among the Q, QH, YQ, and YQH data sets. The relative percentages of 70% P_1* and 30% P_2* are rounded values adopted in Figure 6. The rounded P_1* and P_2* lifetimes are 40 and 130 ps, respectively, in Q and QH and 20 and 130 ps, respectively, in YQ and YQH. Finally, the average overall observed yields of $P^+H_M^-$ are 18% in Q and QH and 34% in YQ and YQH (average values taken from Table 2). Because the 30% P_2* population (130 ps lifetime) undergoes little if any charge separation, the experimentally observed 18% yield of $P^+H_M^-$ in Q and QH and the 34% yield in YQ and YQH, derive entirely from the 70% P_1* fraction. Thus, the decay of P_1* (40 ps lifetime) in Q and QH must be partitioned 26% via ET to H_M and 74% internal conversion to the ground state. In this way, the observed overall 18% yield of $P^+H_M^-$ in Q and QH is obtained (26% × 0.7 ≈ 18%). Similarly, P_1* decay (20 ps lifetime) in YQ and YQH must be partitioned 49% ET to H_M and 51% internal conversion to the ground state, thus giving the overall observed 34% yield of $P^+H_M^-$ for YQ and YQH (49% × 0.7 ≈ 34%).

The partitioning of relative yields of ET (ϕ_{ET}) and ground state recovery (ϕ_{GS}) from P_1*, together with the observed lifetimes (τ_{P1}), allow calculation of the time constants for the respective processes via the expressions $\tau_{ET} = \tau_{P1}/\phi_{ET}$ and $\tau_{GS} = \tau_{P1}/\phi_{GS}$. Because the P_2* fraction for each RC decays by ground state recovery ($\phi_{GS} \approx 1$), the time constant is simply the 130 ps lifetime of P_2*. The values for the time constants thus calculated are shown in Figure 6 for all four mutants. Our results show that Tyr at L181 increases the rate of ET to H_M in YQ, YQH, and YLQ by about 4-fold compared to the native F(L181) present in Q, QH, LQ, and DQ. This finding is expected based on early theoretical predictions[21,41] and previous experimental work[4,8,10,13,42,43] wherein the effects of combinations of Tyr and Phe at L181 and M208 are discussed. In short, Tyr at L181 is expected to preferentially lower the free energy of state $P^+B_M^-$ and thereby enhance ET to the M-side of the RC.

Discussion of P* Populations and Decay Pathways. Complex kinetic profiles of P* decay, obtained using time-resolved absorption and fluorescence spectroscopies, in WT and numerous mutant RCs are well-known. Examples include the following: (i) detection-wavelength-dependent time constants for P* → $P^+H_L^-$ and $P^+H_L^-$ → $P^+Q_A^-$ ET in WT[44,45] and mutants[11,46] at room and low temperature; (ii) excitation-wavelength dependent P-bleaching kinetics;[47−49] and (iii) bi- or multiexponential P* stimulated emission[17,50−56] and spontaneous fluorescence[37,54,57−60] decays. Various models have been discussed including static distributions of RC forms or models invoking dynamic heterogeneity and motions of the chromophores and/or protein.[50,51,61−67]

We have proposed here a coexistence of P* populations (P_1* and P_2*). While likely an oversimplification, this provides some insight into average photophysics/photochemistry and has proved a useful model in previous similar cases.[4,11−13] Differing P* populations (i.e., forms of P* that do not interconvert on the picosecond time scale) could arise from RCs that differ in cofactor−cofactor distances, cofactor−protein interactions, or similar factors that change either the electronic couplings or the small free energy gaps between P* and the charge-separated states. The combination of these factors controls the rates of ET or the ability to do ET at all. Most previous cases where a 30−40% fraction of effectively "inactive" RCs at 285 K was observed have employed changes of the Phe/Tyr pair at L181/M208).[4,12] In two instances, inactive RCs were not present at 285 K but manifested upon cooling the sample to 77 K.[11,13]

dx.doi.org/10.1021/jp305276m | J. Phys. Chem. B 2012, 116, 9971−9982

This observation argues against inactive RCs being a decomposition byproduct of RC isolation procedures.

Although there is consistency among these observations, the details of the molecular origins by which ET is rendered sufficiently slow so as to be ineffective compared to a 100−200 ps internal conversion in a fraction of P* remains unclear. One can imagine many candidate factors such as positioning of water, lipid, or detergent molecules around the pigments; changes in hydrogen bonds; or larger structural changes, to name a few. Such changes may accompany the absence of the B_L in the I(M204)Q-based mutants studied here, and perhaps even disfavor M-side ET in the inactive population. An X-ray structure of a mutant that lacks the H_M cofactor is relevant, and interestingly shows essentially a void in the H_M binding site and no large changes otherwise.[35]

Figure 10 presents free energy level diagrams that can serve as a framework for discussing ET to H_M in the photoactive

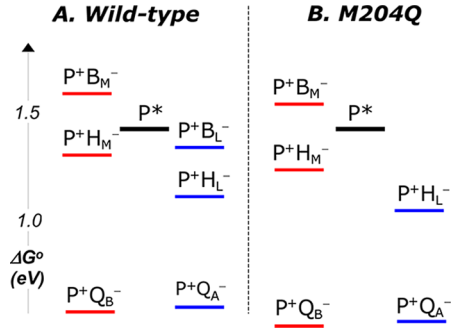

Figure 10. Proposed relative free energies of P* and the charge-separated states in WT (A) and I(M204Q)-based (B) RCs. The free energies of the charge-separated states are not measured directly but placed lower in free energy relative to P* in M204Q than in WT in accord with the measured lower oxidation potential of P in M204Q. The I(M204)Q mutation may have additional effects on, for example, the reduction potential of H_L. See text for further details and proposed effects of other mutations incorporated here, such as L(M212)H and F(L181)Y.

population in Q, QH, YQ, and YQH. Compared to WT (Figure 10A), the free energies of the analogous charge-separated states for I(M204Q)-based RCs (Figure 10B) are ∼50 mV lower. This shift reflects the fact that P is ∼50 mV easier to oxidize in I(M204)Q-based mutants compared to WT (Table 1). In WT, $P^+B_M^-$ is believed to lie above P* by no more than ∼200 mV.[8,21,27,41,68] Other things being equal, the ∼150 ps time constant for P* → $P^+H_M^-$ ET in Q and QH (P_1* fraction; Figure 6) suggests that $P^+B_M^-$ is still above P* in these two mutants. In previous RCs where Tyr at L181 has been used to enhance ET to H_M, the time constant determined for P* → $P^+H_M^-$ has fallen in the range of ∼40−80 ps.[5,7,8,42,43] A similar result is obtained here, namely $\tau_{ET} \approx 40$ ps in YQ and YQH (Figure 6). Calculations have indicated that changing the native Phe to Tyr at L181 will lower the free energy of $P^+B_L^-$ by as much as ∼200 mV.[21] Here and for the previous mutants having Tyr at L181, although it is not known where $P^+B_M^-$ is in free energy with respect to P*, ET is clearly faster compared to RCs having the native Phe at L181.

The dynamics of inherent P* internal conversion in the two populations (Figure 6) is a final point of interest in the I(M204)Q-based mutants. Finding different values for τ_{GS} in the two populations here is an unusual result, with the 40−50 ps value obtained in the photoactive population notably smaller than ∼130 ps in the inactive fraction and the 180−200 ps values measured previously for a variety of RCs in Deriphat at 285 K. For example, in the D_{LL} mutant, the inherent P* time constant for internal conversion at 285 K is 180−200 ps for RCs in chromatophores or isolated with Deriphat and ∼100 ps for RCs in LDAO,[10] the latter value identical to that found for other mutants in LDAO.[5,8] Because no ET occurs in the D_{LL} mutant, the time constant for P* internal conversion to the ground state is simply given by these P* lifetimes. Similarly, in all previous studies of RCs where nominally ET active and inactive P* populations have been observed at 285 K in Deriphat, a 180−200 ps value for P* internal conversion has been characteristic of both populations.[4,10,12,13]

The notable deviation from this trend is the 40−50 ps time constant for internal conversion of P_1* in the I(M204)Q-based RCs studied here. An interesting comparison between the photochemistry in the P_1* population of YQ and YQH, and the photochemistry in a variant of D_{LL} denoted D_{LL}-1,[4] (previously denoted MFLFY[10]) is illustrative. D_{LL}-1 and YQ and YQH have several properties in common. First, in all three RCs the only process with which ET to H_M competes is P* internal conversion. In D_{LL}-1, ET to B_L is not observed and H_L is absent, and in YQ and YQH B_L is absent and ET to H_L (or β_L) is not observed. Second, all three RCs have Tyr at L181. Third, the P/P^+ potentials are similar, with P ∼30 mV easier to oxidize in D_{LL}-1 than WT and ∼50 mV easier to oxidize in YQ and YQH. In D_{LL}-1 the P* lifetime is ∼55 ps and the observed yield of $P^+H_M^-$ is ∼70%. These values determine a 78-ps time constant for P* ET to H_M and a time constant of 183 ps for P* internal conversion to the ground state. Thus, even though the time constant for P* → $P^+H_M^-$ ET in the active P_1* fraction in YQ and YQH is 41 ps, almost a factor of 2 smaller than in D_{LL}-1, the yield of $P^+H_M^-$ is lower (49%) because the P* internal conversion time constant of 39 ps is about a factor of 4 smaller than in D_{LL}-1. In Q and QH, the internal conversion time constant of 54 ps obtained for the P_1* population is similar to that of YQ and YQH (Figure 6). Although the TA data for LQ, DQ, and YLQ were not analyzed to same level of detail, the P* decay profiles and the overall yields of P* → $P^+H_M^-$ ET and P* → P are consistent with rapid P* internal conversion in the active P* population in these mutants as well.

Heterodimer mutants also display fast internal conversion. In heterodimer RCs, the native BChl−BChl dimer P is replaced with a BPh-BChl dimer called D.[69,70] The *Rb. capsulatus* heterodimer-containing H(M200)L and H(L173)L mutants in Deriphat buffer have time constants for D* internal conversion of 27 and 32 ps.[71] The faster internal conversion in the heterodimer compared to the native homodimer is thought to derive from increased contributions from the intradimer charge-transfer configurations $P_L^+P_M^-$ and $P_L^-P_M^+$ to the nature of the excited dimer (P* or D*).[72] In other words, *increased* electronic asymmetry results in a *decreased* internal conversion time constant in heterodimer mutants. The same effect may be responsible for faster P* internal conversion in the I(M204)Q-based RCs, derived from a decrease in symmetry of the environment around P due to the removal of B_L.

AUTHOR INFORMATION

Corresponding Author

*E-mail: kirmaier@wustl.edu. Phone: 314-935-6480. Fax: 314-935-4481.

Notes

The authors declare no competing financial interest.

■ ACKNOWLEDGMENTS

The authors thank the National Science Foundation for supporting this work: Grant MCB-0948996 to C.K. and D.H. and Grant MCB-0918782 to S.G.B.

■ REFERENCES

(1) Zinth, W.; Wachtveitl, J. *ChemPhysChem* **2005**, *6*, 871−880.
(2) Kakitani, Y.; Hou, A.; Miyasako, Y.; Koyama, Y.; Nagae, H. *Chem. Phys. Lett.* **2010**, *492*, 142−149.
(3) Robles, S. J.; Breton, J.; Youvan, D. C. *Science* **1990**, *248*, 1402−1405.
(4) Carter, B.; Boxer, S. G.; Holten, D.; Kirmaier, C. *Biochemistry* **2009**, *48*, 2571−2573.
(5) Heller, B. A.; Holten, D.; Kirmaier, C. *Science* **1995**, *269*, 940−945.
(6) Kellogg, E. C.; Kolaczkowski, S.; Wasielewski, M. R.; Tiede, D. M. *Photosynth. Res.* **1989**, *22*, 47−59.
(7) Kirmaier, C.; Weems, D.; Holten, D. *Biochemistry* **1999**, *38*, 11516−11530.
(8) Kirmaier, C.; He, C.; Holten, D. *Biochemistry* **2001**, *40*, 12132−12139.
(9) Wakeham, M. C.; Jones, M. R. *Biochem. Soc.* **2005**, *133*, 851−857.
(10) Chuang, J. I.; Boxer, S. G.; Holten, D.; Kirmaier, C. *Biochemistry* **2006**, *45*, 3845−3851.
(11) Chuang, J. I.; Boxer, S. G.; Holten, D.; Kirmaier, C. *J. Phys. Chem. B* **2008**, *112*, 5487−5499.
(12) Kirmaier, C.; Laible, P. D.; Hinden, E.; Hanson, D. K.; Holten, D. *Chem. Phys.* **2003**, *294*, 305−318.
(13) Kirmaier, C.; Holten, D. *J. Phys. Chem. B* **2009**, *113*, 1132−1142.
(14) Koepke, J.; Krammer, E. M.; Klingen, A. R.; Sebban, P.; Ullmann, G. M.; Fritzsch, G. *J. Mol. Biol.* **2007**, *371*, 396−409.
(15) Shochat, S.; Gast, P.; Hoff, A. J.; Boender, G. J.; Vanleeuwen, S.; Vanliemt, W. B. S.; Vijgenboom, E.; Raap, J.; Lugtenburg, J.; Degroot, H. J. M. *Spectrochim. Acta A* **1995**, *51*, 135−144.
(16) Nagarajan, V.; Parson, W. W.; Gaul, D.; Schenck, C. *Proc. Natl. Acad. Sci. U.S.A.* **1990**, *87*, 7888−7892.
(17) Chan, C.-K.; Chen, L. X.-Q.; DiMagno, T. J.; Hanson, D. K.; Nance, S. L.; Schiffer, M.; Norris, J. R.; Fleming, G. R. *Chem. Phys. Lett.* **1991**, *176*, 366−372.
(18) Nagarajan, V.; Parson, W. W.; Davis, D.; Schenck, C. C. *Biochemistry* **1993**, *32*, 12324−12336.
(19) Parson, W. W.; Warshel, A. *J. Am. Chem. Soc.* **1987**, *109*, 6152−6163.
(20) Note that the position of this single hydrogen atom is not seen in the highest resolution X-ray structures and no information on this position is available from solid-state NMR.
(21) Alden, R. G.; Parson, W. W.; Chu, Z. T.; Warshel, A. *J. Phys. Chem.* **1996**, *100*, 16761−16770.
(22) Laible, P. D.; Kirmaier, C.; Udawatte, C. S. M.; Hofman, S. J.; Holten, D.; Hanson, D. K. *Biochemistry* **2003**, *42*, 1718−1730.
(23) Andrews, S. S.; Boxer, S. G. *Rev. Sci. Instrum.* **2000**, *71*, 3567−3569.
(24) van der Rest, M.; Gingras, G. *J. Biol. Chem.* **1974**, *249*, 6446−6453.
(25) Kirmaier, C.; Holten, D. *Photosynth. Res.* **1987**, *13*, 225−260.
(26) *Low Temperature Linear Dichroism Study of the Orientation of the Pigments in Reduced and Oxidized Reaction Centers of Rps. viridis and Rb. sphaeroides*; Breton, J., Ed.; Plenum: New York, 1988; pp 59−69.
(27) Katilius, E.; Turanchik, T.; Lin, S.; Taguchi, A. K. W.; Woodbury, N. W. *J. Phys. Chem. B* **1999**, *103*, 7386−7389.
(28) Katilius, E.; Babendure, J. L.; Lin, S.; Woodbury, N. W. *Photosynth. Res.* **2004**, *81*, 165−180.
(29) King, B. A.; McAnaney, T. B.; deWinter, A.; Boxer, S. G. *J. Phys. Chem. B* **2000**, *104*, 8895−8902.
(30) Kirmaier, C.; Gaul, D.; DeBey, R.; Holten, D.; Schenck, C. C. *Science* **1991**, *251*, 922−927.
(31) Nabedryk, E.; Allen, J. P.; Taguchi, A. K. W.; Williams, J. C.; Woodbury, N. W.; Breton, J. *Biochemistry* **1993**, *32*, 13879−13885.
(32) Kirmaier, C.; Cua, A.; He, C.; Holten, D.; Bocian, D. F. *J. Phys. Chem. B* **2002**, *106*, 495−503.
(33) Ridge, J. P.; van Brederode, M. E.; Goodwin, M. G.; van Grondelle, R.; Jones, M. R. *Photosynth. Res.* **1999**, *59*, 9−26.
(34) Moore, L. J.; Boxer, S. G. *Photosynth. Res.* **1998**, *55*, 173−180.
(35) Watson, A. J.; Fyfe, P. K.; Frolov, D.; Wakeham, M. C.; Nabedryk, E.; Van Grondelle, R.; Breton, J.; Jones, M. R. *Biochim. Biophys. Acta* **2005**, *1710*, 34−46.
(36) Leonova, M. M.; Vasilieva, L. G.; Khatypov, R. A.; Boichenko, V. A.; Shuvalov, V. A. *Biochemistry (Moscow)* **2009**, *74*, 452−460.
(37) Jia, Y.; DiMagno, T. J.; Chan, C.-K.; Wang, Z.; Du, M.; Hanson, D. K.; Schiffer, M.; Norris, J. R.; Fleming, G. R.; Popov, M. S. *J. Phys. Chem.* **1993**, *97*, 13180−13191.
(38) Lin, X.; Murchison, H. A.; Nagarajan, V.; Parson, W. W.; Allen, J. P.; Williams, J. C. *Proc. Natl. Acad. Sci. U.S.A.* **1994**, *91*, 10265−10269.
(39) Allen, J. P.; Williams, J. C. *J. Bioenerg. Biomembr.* **1995**, *27*, 275−283.
(40) Kee, H. L.; Laible, P. D.; Bautista, J. A.; Hanson, D. K.; Holten, D.; Kirmaier, C. *Biochemistry* **2006**, *45*, 7314−7322.
(41) Parson, W. W.; Chu, Z. T.; Warshel, A. *Biochim. Biophys. Acta* **1990**, *1017*, 251−272.
(42) Kirmaier, C.; Laible, P. D.; Czarnecki, K.; Hata, A. N.; Hanson, D. K.; Bocian, D. F.; Holten, D. *J. Phys. Chem. B* **2002**, *106*, 1799−1808.
(43) Kirmaier, C.; Laible, P. D.; Hanson, D. K.; Holten, D. *J. Phys. Chem. B* **2004**, *108*, 11827−11832.
(44) Kirmaier, C.; Holten, D. *Proc. Natl. Acad. Sci. U.S.A.* **1990**, *97*, 3522−3556.
(45) Kirmaier, C.; Holten, D.; Parson, W. W. *Biochem. Biophys. Acta* **1985**, *810*, 33−48.
(46) Williams, J. C.; Alden, R. G.; Murchison, H. A.; Peloquin, J. M.; Woodbury, N. W.; Allen, J. P. *Biochemistry* **1992**, *31*, 11029−11037.
(47) Peloquin, J. M.; Lin, S.; Taguchi, A. K. W.; Woodbury, N. W. *J. Phys. Chem.* **1995**, *99*, 1349−1356.
(48) Peloquin, J. M.; Lin, S.; Taguchi, A. K. W.; Woodbury, N. W. *J. Phys. Chem.* **1996**, *100*, 1428−14235.
(49) Lin, S.; Jackson, J.; Taguchi, A. K. W.; Woodbury, N. W. *J. Phys. Chem. B* **1998**, *102*, 4016−4022.
(50) Vos, M. H.; Lambry, J. C.; Robles, S. J.; Youvan, D. C.; Breton, J.; Martin, J. L. *Proc. Natl. Acad. Sci. U.S.A.* **1991**, *88*, 8885−8889.
(51) Vos, M. H.; Lambry, J. C.; Robles, S. J.; Youvan, D. C.; Breton, J.; Martin, J. L. *Proc. Natl. Acad. Sci. U.S.A.* **1992**, *89*, 613−617.
(52) Taguchi, A. K.; Stocker, J. W.; Alden, R. G.; Causgrove, T. P.; Peloquin, J. M.; Boxer, S. G.; Woodbury, N. W. *Biochemistry* **1992**, *31*, 10345−10355.
(53) Beekman, L. M. P.; van Stokkum, I. H. M.; Monshouwer, R.; Rijnders, A. J.; McGlynn, P.; Visschers, R. W.; Jones, M. R.; van Grondelle, R. *J. Phys. Chem.* **1996**, *100*, 7256−7268.
(54) Laible, P. D.; Greenfield, S. R.; Wasielewski, M. R.; Hanson, D. K.; Pearlstein, R. M. *Biochemistry* **1997**, *36*, 8677−8685.
(55) Beekman, L. M. P.; Visschers, R. W.; Monshouwer, R.; Heer-Dawson, M.; Mattioli, T. A.; McGlynn, P.; Hunter, C. N.; Robert, B.; Van Stokkum, I. H. M.; Van Grondelle, R.; Jones, M. R. *Biochemistry* **1995**, *34*, 14712−14721.
(56) Huppman, P.; Arlt, T.; Penzkofer, H.; Schmidt, S.; Bibikova, M.; Dohse, B.; Oesterhelt, D.; Wachtveit, J.; Zinth, W. *Biophys. J.* **2002**, *82*, 3186−3197.
(57) Du, M.; Rosenthal, S. J.; Xie, X.; DiMagno, T. J.; Schmidt, M.; Hanson, D. K.; Schiffer, M.; Norris, J. R.; Fleming, G. R. *Proc. Natl. Acad. Sci. U.S.A.* **1992**, *89*, 8517−8521.
(58) Hamm, P.; Gray, K. A.; Oesterhelt, D.; Feick, R.; Scheer, H.; Zinth, W. *Biochim. Biophys. Acta* **1993**, *1142*, 99−105.
(59) Stanley, R. J.; Boxer, S. G. *J. Phys. Chem.* **1995**, *99*, 859−863.

(60) Muller, M. G.; Griebenow, K.; Holzarth, A. R. *Chem. Phys. Lett.* **1992**, *199*, 465−469.
(61) Lin, S.; Taguchi, A. K. W.; Woodbury, N. W. *J. Phys. Chem.* **1996**, *42*, 17067−17078.
(62) Peloquin, J. M.; Williams, J. C.; Lin, X.; Alden, R. G.; Taguchi, A. K. W.; Allen, J. P.; Woodbury, N. W. *Biochemistry* **1994**, *33*, 8089−8100.
(63) Woodbury, N. W.; Peloquin, J. M.; Alden, R. G.; Lin, X.; Lin, S.; Taguchi, A. K. W.; Williams, J. C.; Allen, J. P. *Biochemistry* **1994**, *33*, 8101−8112.
(64) Wang, H. Y.; Lin, S.; Allen, J. P.; Williams, J. C.; Blankert, S.; Laser, C.; Woodbury, N. W. *Science* **2007**, *316*, 747−750.
(65) Holzwarth, A. R.; Muller, M. G. *Biochemistry* **1996**, *35*, 11802−11831.
(66) Gehlen, J. N.; Marchi, M.; Chandler, D. *Science* **1994**, *263*, 499−502.
(67) Bixon, M.; Jortner, J.; Michel-Beyerle, M. E. *Chem. Phys.* **1995**, *197*, 389−404.
(68) Gunner, M. R.; Nicholls, A.; Honig, B. *J. Phys. Chem.* **1996**, *100*, 4277−4291.
(69) Bylina, E. J.; Youvan, D. C. *Proc. Natl. Acad. Sci. U.S.A.* **1988**, *85*, 7226−7230.
(70) Kirmaier, C.; Holten, D.; Bylina, E. J.; Youvan, D. C. *Proc. Natl. Acad. Sci. U.S.A.* **1988**, *85*, 7562−7566.
(71) Kirmaier, C.; Bautista, J. A.; Laible, P. D.; Hanson, D. K.; Holten, D. *J. Phys. Chem. B* **2005**, *109*, 24160−24172.
(72) McDowell, L. M.; Kirmaier, C.; Holten, D. *Biochem. Biophys. Acta* **1990**, *1020*, 239−246.